A High-Resolution Numerical Modeling Study of the Subtidal Circulation in the Northern South China Sea

David C. Chapman, Dong-Shan Ko, and Ruth H. Preller

Abstract—**A high-resolution, regional, numerical-model-based, real-time ocean prediction system for the northern South China Sea, called the Northern South China Sea Nowcast/Forecast System (NSCSNFS), has been used to investigate subtidal mesoscale flows during the time period of the Asian Seas International Acoustic Experiment (ASIAEX) field programs. The dynamics are dominated by three influences; 1) surface wind stress, 2) intrusions of the Kuroshio through Luzon Strait, and 3) the large-scale cyclonic gyre that occupies much of the northern South China Sea. Each component primarily drives currents in the upper ocean, so deep currents are rather weak. Wind stress is especially effective at forcing currents over the shallow China shelf. The Kuroshio intrusion tends to flow westward until it meets the northern edge of the large-scale cyclonic gyre. Together, these currents produce an intense, narrow jet directed northwest toward the continental slope, often in the region of the ASIAEX field programs. Upon reaching the slope, the current splits with part flowing northeastward along the slope and part flowing southwestward, producing large horizontal and vertical shears and making this region dynamically very complicated and difficult to simulate. The Kuroshio intrusion tends to be stronger (weaker) when the northeasterly winds are strong (weak) and the large-scale gyre is farther south (north), consistent with conclusions from previous model studies. At the northern boundary, the model produces a persistent northward flow through Taiwan Strait into the East China Sea. Data assimilation in the NSCSNFS model is shown to dampen the system, extracting energy and causing the entire system to spin down.**

Index Terms—**Asian Seas International Acoustic Experiment (ASIAEX), numerical modeling, ocean dynamics, South China Sea.**

I. Introduction

THE South China Sea (SCS) is a large and deep semi-enclosed marginal sea, located in the western tropical Pacific Ocean; bounded by Asia to the west, the Philippines to the east, Borneo to the south, and Taiwan to the north. The only deep connection between the SCS and the Pacific Ocean is Luzon Strait, located in the northern SCS between the islands of Luzon and Taiwan (see Fig. 1). Taiwan Strait provides a shallow connection between the northern SCS and the East China Sea. The large-scale circulation in the SCS is primarily driven by the monsoonal winds, which are typically from the northeast from October through March and reverse to be from the southwest from June through August. In winter, the winds drive a basin-scale cyclonic gyre, while in summer the winds drive an anticyclonic gyre in the southern SCS and a cyclonic gyre in the Northern SCS [21]. In the northern SCS, the wind-driven circulation is altered by large intrusions of relatively warm and salty Kuroshio water through Luzon Strait. The occurrence and structure of Kuroshio intrusions (i.e., penetration distance, eddy shedding, etc.) are irregular and poorly understood; yet the intrusions have major effects on the circulation in the northern SCS (e.g., [14]).

Numerous investigators have studied various aspects of the dynamics of the circulation within the SCS, often relying on numerical models. For example, Chao *et al.* [5] studied upwelling and downwelling of deep water. Metzger and Hurlburt [18] modeled the upper ocean circulation, showing that the wind curl is important in driving the mean cyclonic flow over most of the SCS. They also showed that the wind plays a significant role in determining the transport through Luzon Strait (i.e., Kuroshio intrusions). More recently, Metzger and Hurlburt [19] studied the driving of Kuroshio intrusions and found that they are largely unpredictable, although the wind curl appears to be related to the intensity of the intrusions. Liu *et al.* [17] concluded that the wind curl basically sets the seasonal variability in the SCS, while Kuroshio intrusions are important only in the northern SCS. The latter result was also obtained by Cai *et al.* [2]. Chern and Wang [7] have recently suggested that Kuroshio intrusions may be regulated by the position of the large-scale wind-driven cyclonic gyre within the SCS. That is, during winter, the gyre is displaced toward the southern SCS, allowing more persistent Kuroshio intrusions. With the reversal of the monsoonal winds during summer, the gyre extends northward and tends to inhibit Kuroshio intrusions.

Taken together, these studies indicate that the northern SCS is a dynamically complex region where at least two highly energetic flows (the large-scale wind-driven cyclonic gyre and Kuroshio intrusions) interact. It is also a region of complex bathymetry, with a broad shallow shelf along the China coast, a steep and irregular continental slope that extends from southwest to northeast nearly to the Taiwan coast, and a deep offshore basin (see Fig. 1). The details of the circulation here, and in particular within the domain of the Asian Seas International Acoustic Experiment (ASIAEX) field programs (small dotted box in Fig. 1), are beyond the resolution of the models mentioned

The work of D. C. Chapman was supported by the Office of Naval Research under Grant N00014-00-1-0210. The work of D. S. Ko and R. H. Preller's was supported through the Office of Naval Research's Ocean Modeling and Prediction Program (Program Element 0602435N). This paper is Woods Hole Oceanographic Institution contribution 11214 and NRL contribution NRL/JA/7320/03/117, which is approved for public release, distribution unlimited.

D. C. Chapman, deceased, was with the Physical Oceanography Department, Woods Hole Oceanographic Institution, Woods Hole, MA 02543 USA.

D.-S. Ko and R. H. Preller are with the Naval Research Laboratory, Stennis Space Center, MS 39529 USA (e-mail: ko@nrlssc.navy.mil).

Digital Object Identifier 10.1109/JOE.2004.838334

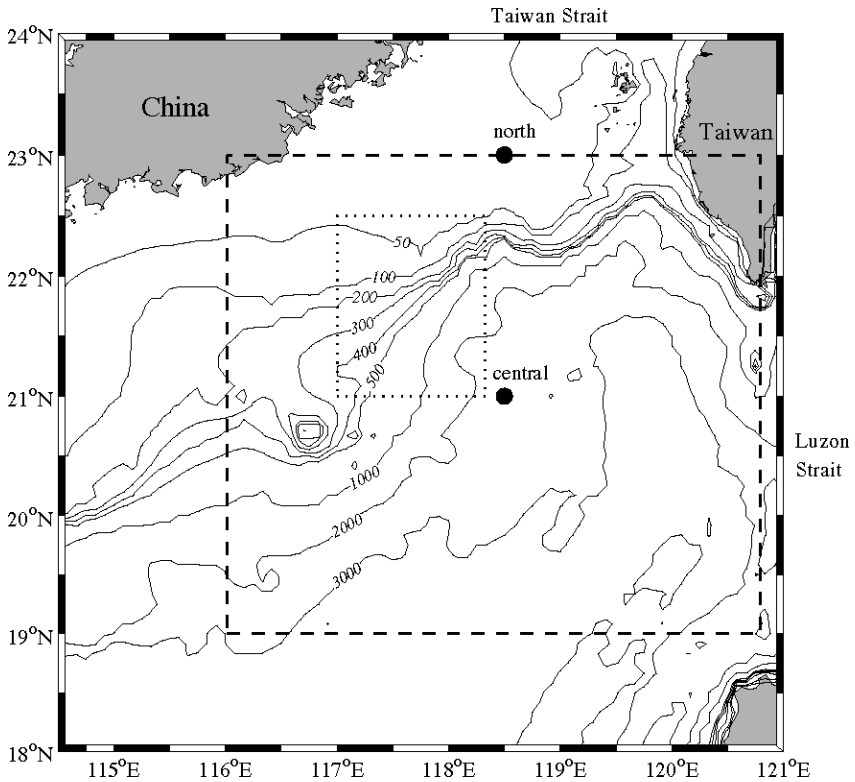

Fig. 1. Map of the northern South China Sea. The large dashed box denotes the area of analysis for the present paper. The small dotted box indicates the region of the ASIAEX field programs. Solid circles show locations of representative wind records presented in Fig. 2.

above, all of which consider the entire SCS (or more). Therefore, the Naval Research Laboratory has undertaken the development of a high-resolution, regional, numerical-model-based, real-time ocean prediction system for the northern SCS called the Northern South China Sea Nowcast/Forecast System (NSCSNFS) that encompasses the domain shown in Fig. 1. This domain was chosen to include the entire area of interest to the ASIAEX field programs at high resolution with open boundaries located along the key straits and far enough away from the area of interest to minimize any influence from the open boundary conditions. (The results of this forecast system were made available to the investigators of the ASIAEX field programs via a website.) The principal advantage of this model is that some dynamical processes can be resolved and modeled more realistically and at smaller scales. The primary disadvantage is that most of the domain boundaries are open, so currents and water properties from outside the model domain must be prescribed in some way. Thus, the model is limited to some extent by the adequacy of these prescriptions.

Given that the model domain includes the area of the ASIAEX field efforts, we have used the NSCSNFS model with three goals in mind; 1) to describe the important mesoscale flows and dynamics that might be observed during the ASIAEX field programs, 2) to examine the sensitivity of the model to various parameters and imposed forcing fields, and 3) to identify model weaknesses that could point to possible improvements. We do not attempt a direct comparison between the NSCSNFS model results and ASIAEX field measurements. Such an undertaking is presently being pursued by other ASIAEX investigators. One important caveat is that the NSCSNFS model considers only subtidal motions, so there are no astronomical tides or tidally generated internal solitary waves that often dominate the higher frequency motions (see other articles in this issue). Such high-frequency flows can greatly complicate the interpretation of large-scale surveys (e.g., Gawarkiewicz *et al.*, this issue).

The NSCSNFS model and its application are described in Section II. The forcing fields used in the model are discussed in Section III. The full-model response is described in Section IV. The results from a number of diagnostic model runs are then used in Section V to better understand the model response. Some discussion and a summary follow in Section VI.

II. NSCSNFS Model Description

The NSCSNFS model is based on the Princeton Ocean Model [1] with 1/24° horizontal resolution and 30 vertical grid points within the model domain shown in Fig. 1. The vertical grid points are concentrated near the surface and bottom in order to resolve the boundary layers. For example, at 200-m total depth there are seven grid points within 12 m of the bottom. At 500-m total depth there are five grid points within 20 m of the bottom. The bottom topography is interpolated to the model grid from the NRL DBDB2, two-minute global topography database. The Navy Operational Global Atmospheric Prediction System (NOGAPS; [20]) provides surface forcing fields to drive the model: wind stress, total heat flux, solar radiation and sea level air pressure. Real-time data, the sea surface height

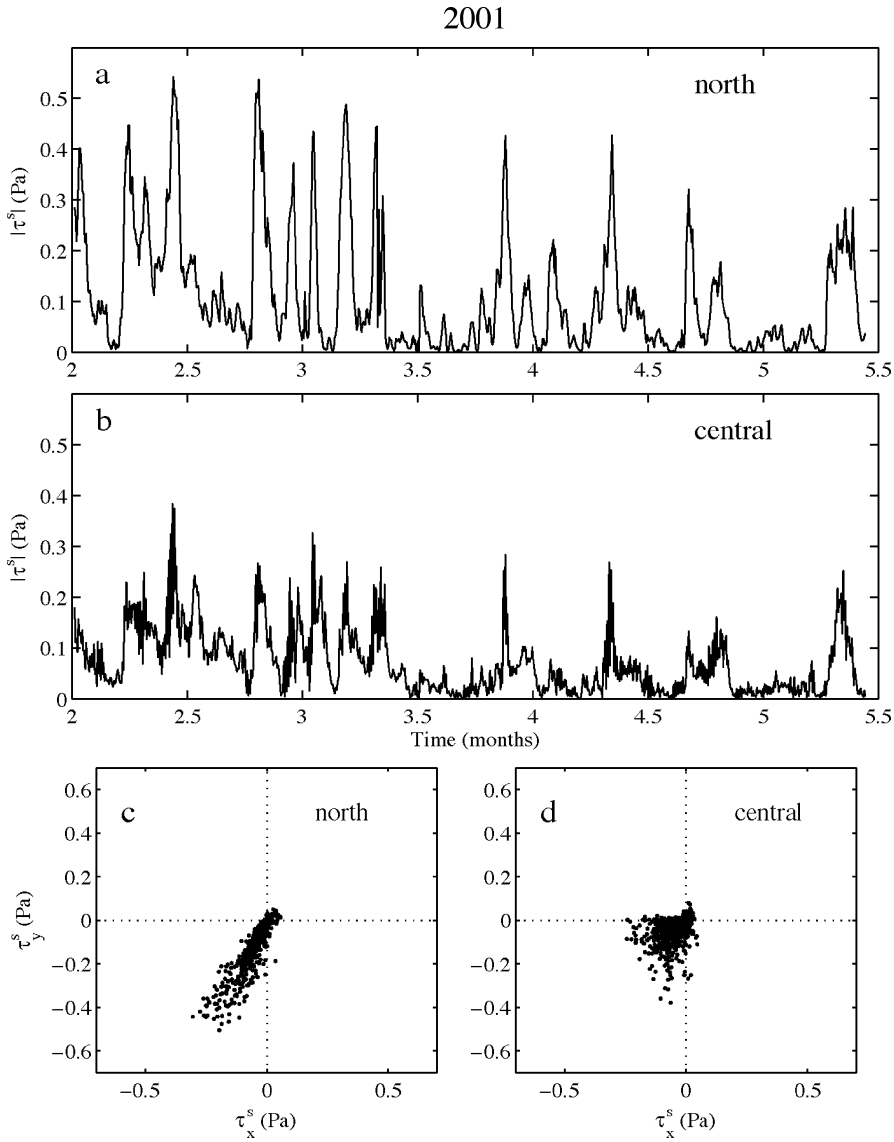

Fig. 2. Wind stress magnitudes (a, b) and directions (c, d) for the two locations marked by solid circles in Fig. 1 during year 2001.

anomalies from altimeters and the MCSST from AVHRR, are assimilated as described in the Appendix. A North Pacific Ocean Nowcast/ Forecast System, similar to the NSCNFS, but encompassing a much larger domain with horizontal resolution of 1/4° [15], provides sea surface height, currents, temperatures and salinities at the open boundaries.

The NSCSNFS model runs continuously, but we are primarily interested in the behavior during the times of the ASIAEX field programs. Therefore, we have limited this study to the period of February 1 to May 15 during both years 2000 and 2001, which captures the transition between winter and summer monsoons, includes the period when the Kuroshio is strong and then weakens, and encompasses the ASIAEX field programs. For convenience, we consider the region within the dashed box in Fig. 1, which encompasses both the large- and small-scale survey areas of ASIAEX. The model behavior was qualitatively quite similar during both years, so most of the results presented are from 2001. Results from 2000 are included when useful.

III. Forcing Fields

The NSCSNFS model responds most readily to the wind stress and flows imposed at the open boundaries, so it is helpful to characterize these forcing fields before proceeding. The wind stress is highly variable in both space and time, but nonetheless fairly easy to describe. Fig. 2 shows the wind stress magnitude and direction at two locations within the model domain (solid dots in Fig. 1), one over the shelf near the northern boundary and one in the center of the study domain. Strong wind events ($|\tau^s| > 0.4$ Pa) occur fairly regularly at the north location until mid-March, when the transition to the summer monsoon begins, after which there are fewer strong storms [see Fig. 2(a)]. The wind at the north location is nearly always from the northeast [see Fig. 2(c)]. The central wind stress is highly visually correlated with the north wind stress, but its magnitude is considerably reduced [see Fig. 2(b)], and its direction is much more variable [see Fig. 2(d)]. These features are typical of the strong wind-stress curl that occurs southwest of Taiwan,

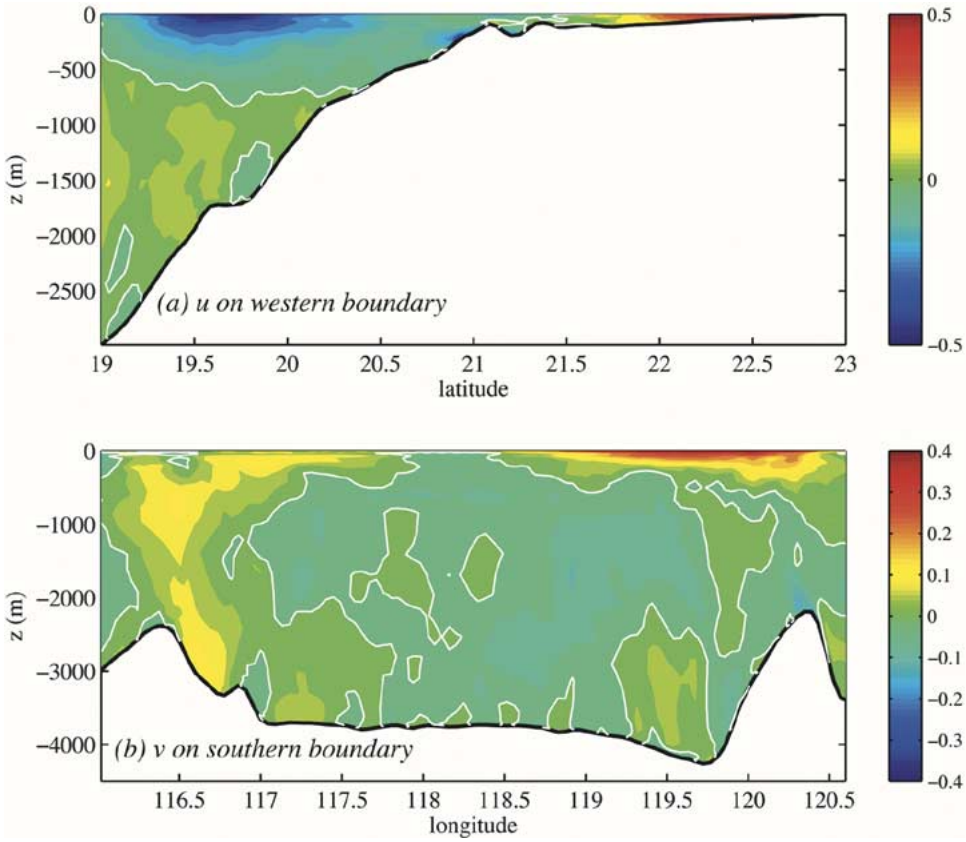

Fig. 3. Vertical sections of velocity normal to (a) the western open boundary and (b) the southern open boundary on March 15 of the 2001 full-model calculation. Velocity scales are shown at the right in ms^{-1}. Positive velocities are out of the page. The white contour is zero velocity.

presumably the result of the island partially blocking the northeast wind. Plots of wind stress at these locations for this period in 2000 are qualitatively identical to Fig. 2. Thus, the wind stress is virtually always from the northeast with a substantial cyclonic curl during strong wind events, and changes direction only during periods of very weak winds.

The flows through the open boundaries are more difficult to generalize, but several features are typical. Transport through the northern boundary (Taiwan Strait) is small (despite strong currents) because of the shallow depths, and is almost always northward, carrying relatively warm, salty water. Flow through the eastern, western and southern boundaries is highly variable in both magnitude and direction, and all three boundaries contribute substantially to cross-boundary exchange. Close examination of nonshelf flows through the western and southern boundaries shows that they tend to be related; i.e., northward inflow at the southern boundary usually occurs with westward outflow through the western boundary. Fig. 3 shows a typical example; at the southern boundary [see Fig. 3(b)] the near-surface flow is almost entirely northward (yellow and red, into the model domain), while at the western boundary [see Fig. 3(a)] the near-surface flow in the deeper regions is westward (blue, out of the model domain). This flow is to be expected when the large-scale, wind-driven cyclonic SCS gyre (described in the introduction) moves into the model domain. It will tend to carry relatively cold, fresh water in through the southern boundary and out through the western boundary. Notice that the shelf flow through the western boundary [see Fig. 3(a)] is eastward (red, into the model domain), consistent with the northward outflow through Taiwan Strait.

Flow through the eastern boundary is dominated by Kuroshio intrusions, which typically provide a net influx of relatively warm, salty Kuroshio water to the model domain. Fig. 4 shows a typical example; a strong inflow (blue) occurs between $20^{\circ}\mathrm{N}$ and $21^{\circ}\mathrm{N}$ in Fig. 4(a), extending to about 400 m depth. The maximum inflow velocity of about 0.5 ms^{-1} occurs at slightly less than 100 m depth. A somewhat weaker outflow (maximum of about 0.2 ms^{-1}) is found just south of Taiwan, centered at about $21.7^{\circ}\mathrm{N}$.

At all of the open boundaries, most of the flow is limited to relatively shallow depths ($<$400 m). That is, as in Figs. 3 and 4, the most energetic flows occur in the upper ocean, providing the bulk of the mass and momentum flux into and out of the domain. Flows at greater depths are very weak. The model response to other forcing fields (e.g. surface heat flux, atmospheric pressure) is extremely weak during the time period considered here, so these fields are not summarized.

IV. Full-Model Response

The NSCSNFS model response with full forcing is described in this section. The model calculation begins on February1, using the full-model operational forecast for that day as the initial condition. An overview of the dominant flow patterns is provided by several snapshots of surface salinity and horizontal velocities, each separated by one month during the 2001 period

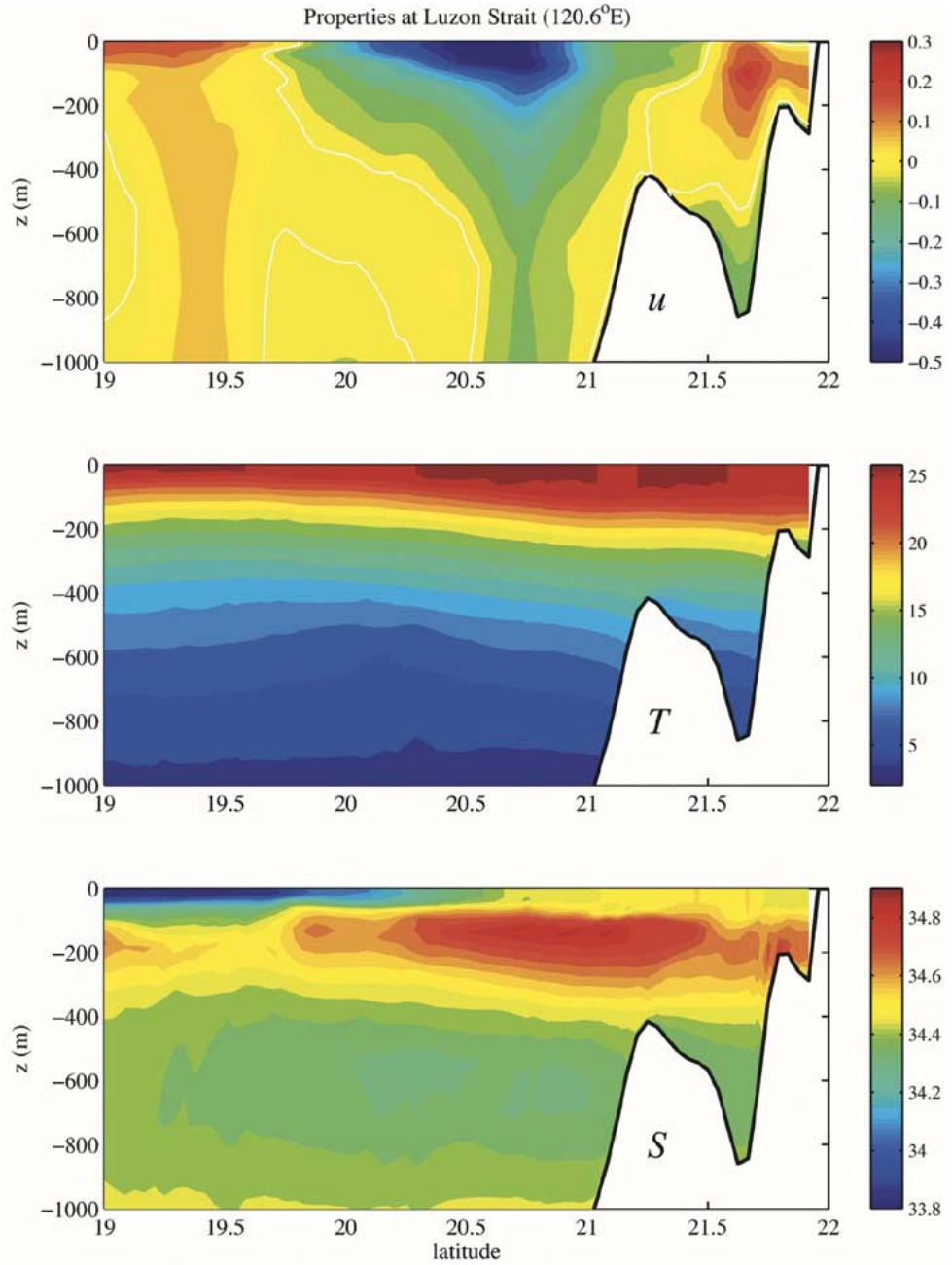

Fig. 4. Vertical sections of (a) east-west velocity (ms^{-1}), (b) temperature $(^{\circ}\mathrm{C})$, and (c) salinity (psu) in the upper 1000 m at Luzon Strait (120.6° E) on February 1 of the 2001 full-model calculation. Scales are shown at the right. Positive velocities are out of the page. The white contour in (a) is zero velocity.

(see Fig. 5). Here salinity acts as a nearly passive tracer because temperature essentially determines the density. For reference, the white region in the northeast corner is the southwestern part of Taiwan, while the tiny white patch in the northwest corner is the coast of China (see Fig. 1).

The flow patterns typically have fairly large scales, especially in the deep basin. This is to be expected because the baroclinic Rossby radius is about 45 km over most of the deep basin. (The baroclinic Rossby radius is computed as the first-baroclinic-mode phase speed divided by the Coriolis parameter.) Thus, eddies formed in the deep basin by geostrophic adjustment or baroclinic instabilities, for example, should have diameters of roughly 150–200 km.

There are three basic features of the flow, each present in the February 15 snapshot [see Fig. 5(a)]. First, a strong Kuroshio intrusion through the eastern boundary carries relatively salty water (up to 34.6 psu) into the domain. Second, a large-scale inflow of relatively fresh water enters through the southern boundary, turns westward and exits through the western boundary. This is the northern edge of the large-scale, wind-driven SCS gyre discussed extensively by Chern and Wang [7]. These two water masses meet to form a strong jet flowing toward the northwest that splits upon reaching the continental slope, with some flow moving eastward along the slope toward Taiwan and some flowing westward. Notice that the current splits near 118°E and 21°N, which is close to where

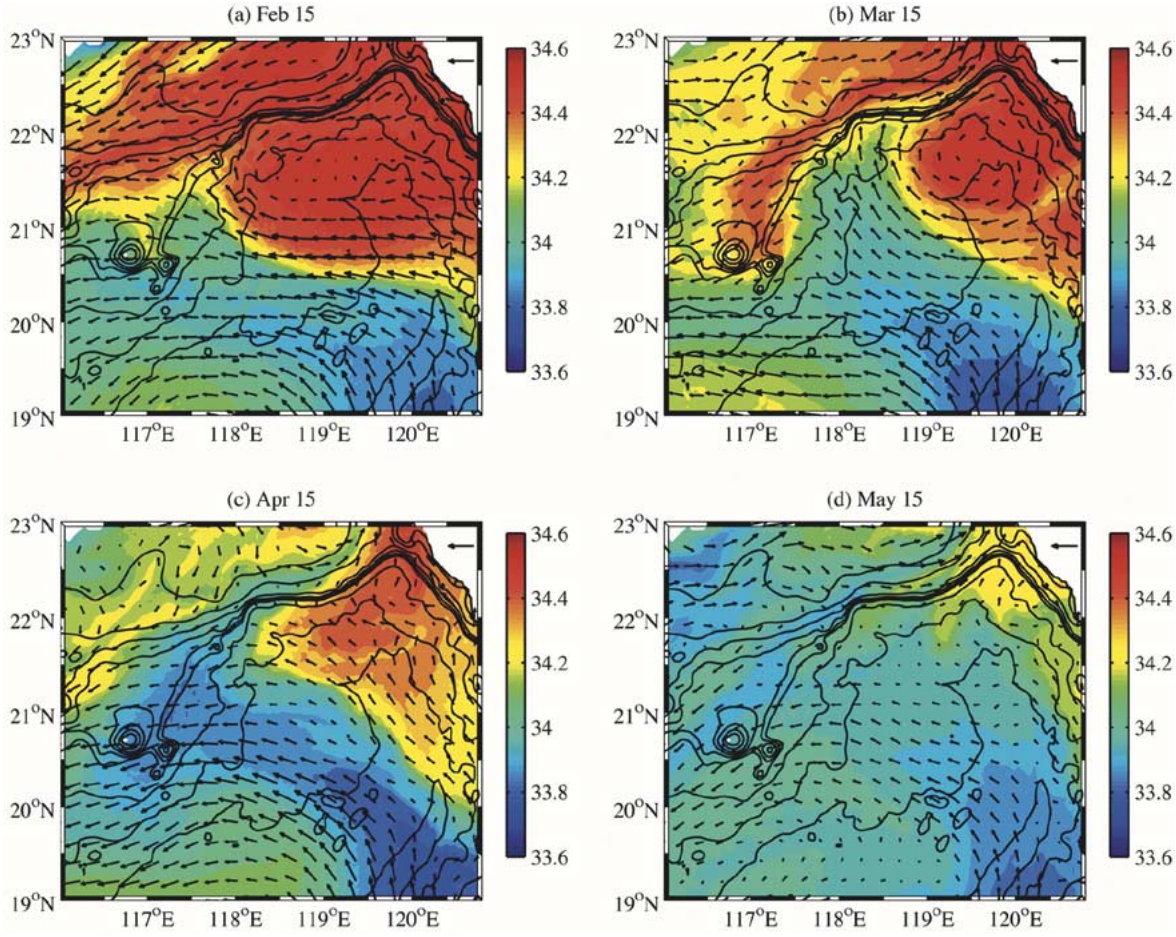

Fig. 5. Surface velocity vectors and salinity at four times during the 2001 full-model calculation. The vector scale plotted on Taiwan is 0.5 ms^{-1}. Salinity scale is shown at the right in psu. Black contours show the 50, 100, 200, 300, 400, 500, 1000, 2000, 3000, and 4000 m isobaths. (a) February 15; (b) March 15; (c) April 15; (d) May 15.

the small-scale ASIAEX field programs took place, suggesting that the regional flows there are intrinsically complicated. The third basic feature is the wind-driven flow on the China shelf (northwestern part of the model domain). The February 15 snapshot occurs during a strong northeasterly wind event (see Fig. 2), and the currents are slightly to the right of the wind stress, as expected for wind-forced shelf flow.

A less pronounced feature of Fig. 5(a) is the northward flow at the northern boundary, just west of Taiwan. This is the principal source of the relatively salty water that persistently exits the model domain through Taiwan Strait, even during strong northeasterly wind events.

Qualitatively, the circulation during the study period for each year can be viewed as a combination of these three flows, changing according to the relative strength of each flow at any particular time. For example, by March 15 [see Fig. 5(b)] the winds have begun to relax, the large-scale gyre has moved northward, and the Kuroshio intrusion has weakened and moved northeast toward the Taiwan coast. Consequently, the point at which the northwestward jet splits has moved northeast along the slope, so the flow in the ASIAEX field programs region is now primarily southwestward. The shelf flow is weak and disorganized in conjunction with the weak winds. As the frequency of strong northeasterly wind events decreases, the shelf flow remains weak and variable, the large-scale gyre continues to move northward, and the Kuroshio intrusion becomes quite small by April 15 [see Fig. 5(c)] and is essentially eliminated by May 15 [Fig. 5(d)].

These flow changes are consistent with the argument by Chern and Wang [7] that the winds control the large-scale gyre position, which in turn controls the Kuroshio intrusion. That is, the winter monsoonal winds push the large-scale gyre to the south, allowing Kuroshio intrusions. As the winds weaken, the gyre moves northward, blocking the Kuroshio intrusions. However, we cannot sort out the cause and effect relationship from this single model run because all forcings are imposed and the inflows at both the southern and eastern boundaries are prescribed (but see Section V-B).

The surface flows in Fig. 5 do not extend deeper than about 400 m, consistent with the boundary flows described in Section III. For example, Fig. 6 shows vertical sections of east-west velocity and density along 118.75°E latitude, through the Kuroshio intrusion seen in Fig. 5(a). Nearly all of the flow is in the upper 400 m, with velocities reaching about 0.5 ms^{-1}. Such shallow flows in the deep basin are typical of all times during both years. The deep flows in the deep basin are always weak.

In order to quantify the strength of the model response in space and time, we have computed the volume-averaged kinetic

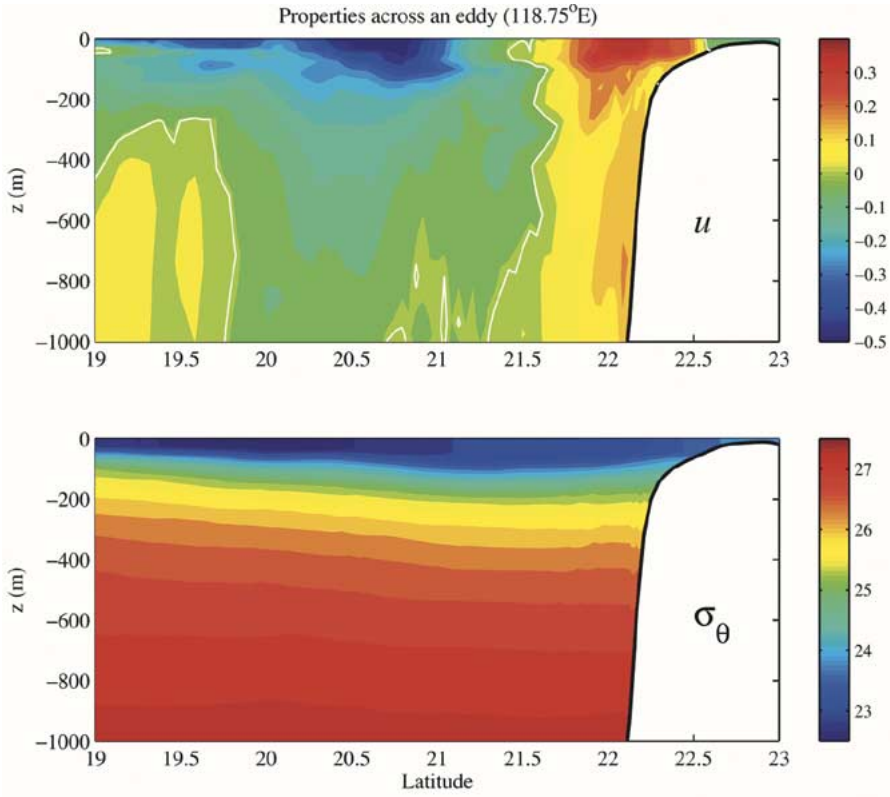

Fig. 6. Vertical sections of (a) east-west velocity (ms^{-1}) and (b) potential density (kgm^{-3}) in the upper 1000 m along longitude 118.75°E for the 2001 full-model calculation. Scales are shown at the right. Positive velocities are out of the page. The white contour in (a) is zero velocity.

energy (KE) in four nonoverlapping parts of the model domain: 1) a shelf region with bottom depth less than 100 m, 2) a slope region with bottom depth greater than 100 m and less than 1000 m, 3) an upper-ocean region between the surface and 400 m, in all regions where the bottom depth is greater than 1000 m, and 4) a deep-ocean region between 400 m and the bottom, in all regions where the bottom depth is greater than 1000 m. The KE for each part, computed at half-month intervals, is shown in Fig. 7 for both years 2000 and 2001.

The KE in the deep-ocean region (squares) is always quite small in both years, as stated above. During both years, the slope region (triangles) and the upper-ocean region (diamonds) have comparable KE that generally decreases with time. The decrease results from the decrease in wind stress during the transition from winter to summer monsoons (e.g., Fig. 2), a weakening of the Kuroshio intrusion in summer, and data assimilation as shown below. These regions are somewhat less energetic during 2001. The shelf region (circles) shows the highest degree of variability with the largest overall KE because it is most sensitive to the direct effects of the wind and the open-boundary throughflows. In particular, the very large shelf KE on 15 March 2001 is caused by the interaction of the Kuroshio intrusion with the shelf/slope just west of Taiwan [see Fig. 5(b)] which produces strong currents at the shelf edge and a swift northward flow through the eastern part of Taiwan Strait. Interestingly, the total flow through Taiwan Strait is not unusually large at this time, but the effect on shelf currents is considerable. The high shelf KE in May of 2001 is caused by a large inflow through the western boundary [see Fig. 3(a)], which occurs almost entirely over the shelf at this particular time, thereby generating unusually strong currents there. The highly variable flows on the shelf suggest that their accurate prediction may be rather difficult.

It was noted above (see Fig. 5) that the ASIAEX field programs were located in a dynamically complex region. Figs. 8 and 9 further emphasize this point. Fig. 8 shows salinity and current vectors in the ASIAEX field program region at the surface and at 100 m depth for two times during 2001. On February 15 [see Fig. 8(a) and (b)], the northwestward jet created by the confluence of the large-scale gyre and the Kuroshio intrusion encounters the continental slope and splits near the middle of the field program region. Currents at the surface and at 100 m are basically in the same direction, i.e., the upper-ocean response is fairly uniform, carrying relatively salty water with somewhat higher salinities at 100 m. This is consistent with the observed maximum salinity of 34.8 at 150 m depth for Kuroshio intrusions [10]. The shelf currents are essentially all toward the southwest, driven by the surface wind stress. However, by May 1 [see Fig. 8(c) and (d)], the northwestward jet has moved to the northeast of the field program region (see Fig. 5), and the flow over most of the region is opposite to that of February 15. Furthermore, surface salinity and currents bear little resemblance to those at 100 m. Surface currents are primarily directed offshore toward the southeast, responding to the wind stress and carrying relatively fresh water. That is, at the surface the effect of the wind stress is now stronger than the influence of the northwestward jet, so the wind stress dominates. Currents at 100 m carry relatively salty Kuroshio water along the slope toward the

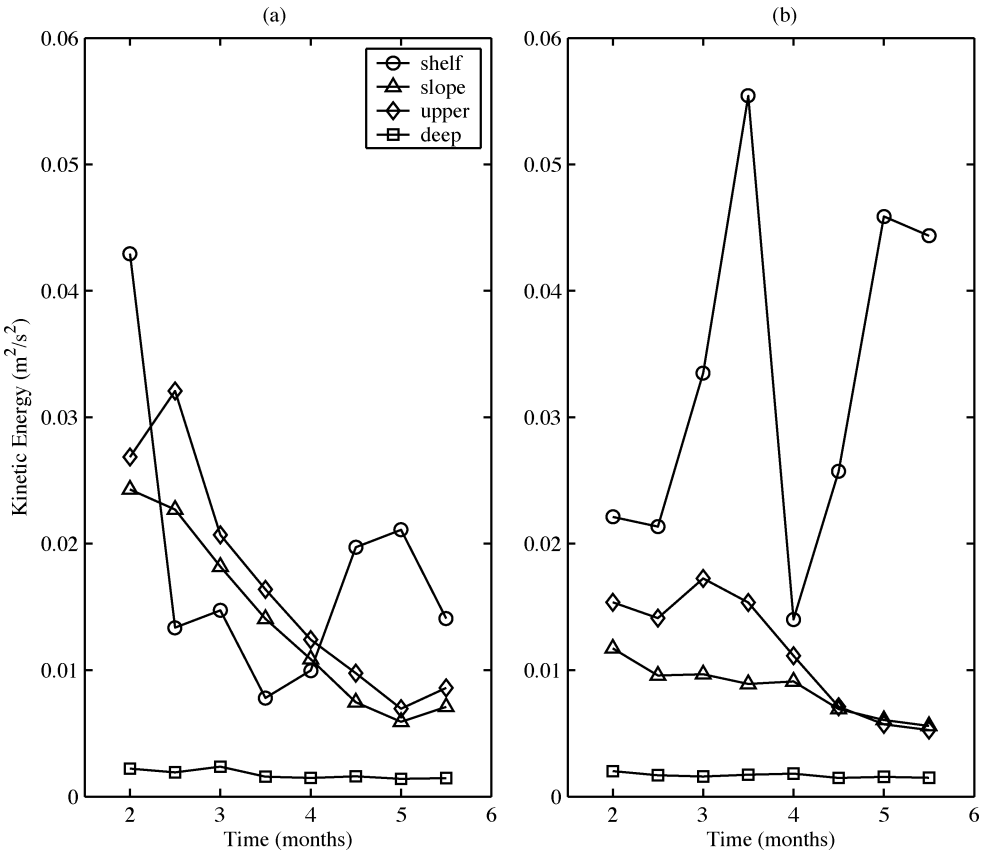

Fig. 7. Time history of the volume-averaged kinetic energy within each of the four nonoverlapping regions (defined in the text) for the full-model calculations in years (a) 2000 and (b) 2001.

southwest, still driven by the northwestward jet, which is now east of this region.

Fig. 9 shows the change in vertical structure of the alongslope currents [normal to the black line in Fig. 8(a)] accompanying the change in location of the northwestward jet. On February 15 [see Fig. 9(a)], the flow is nearly entirely toward the northeast (red). On May 1 [see Fig. 9(b)], the near-surface flow and the flow over the shelf have a northeast component, but the flow over most of the slope (shallower than 800 m) is reversed toward the southwest (blue). These results show that the flow in this region, especially over the shelf and slope, can be highly variable in both space and time, depending on the interaction of the deep basin flows and the wind stress.

A small-scale process that is nicely captured by the NSCSNFS model is the tendency for buoyancy shutdown of the bottom boundary layer in regions of strong stratification over sloping topography (see [9], for an excellent review). That is, alongslope currents produce Ekman transport at the bottom either up or down the slope, carrying buoyancy and tilting isopycnals within the bottom boundary layer. The thermal-wind shear introduced by the horizontal density gradients reduces the velocity at the bottom, thereby decreasing bottom stress. In this way, the flow adjusts to reduce the stress felt by the overlying flow, allowing stratified flow over a sloping bottom to persist much longer than would be anticipated based on standard drag-law estimates of spindown times.

Fig. 10 shows two vertical sections that illustrate buoyancy shutdown for both downwelling and upwelling flows. Downwelling currents [into the page, blue in Fig. 10(a)] generate Ekman transport down the slope. Light water is carried under heavy water, which mixes rapidly to produce a thick bottom boundary layer. The density gradient in the boundary layer is such that the alongslope velocity becomes small near the bottom (white is zero) and even reverses under part of the flow. Notice that the tilting of the isopycnals at the bottom increases as the stratification weakens with depth (say, below 200 m depth) because the thermal-wind shear is less with weaker stratification, so the bottom mixed layer grows thicker before shutdown occurs. In contrast, upwelling currents [out of the page, red in Fig. 10(b)] generate Ekman transport up the slope, carrying denser water under lighter water. The boundary layer thins, but thermal-wind shear still reduces the velocity toward zero at the bottom. In this case, the flow is actually slightly reversed at the bottom over most of the section. Again, the upward tilting of isopycnals is greater at depth where the stratification is weaker, as required to achieve shutdown. Thus, in both sections, buoyancy shutdown has reduced the bottom stress, and consequently the interior flows can maintain for longer times and/or distances.

V. Diagnostic Model Runs

In order to investigate the complex behavior of the operational model, we have rerun the model numerous times for each year in somewhat simpler scenarios. First, a calculation was started from the same initial state as the full model described above (the full NSCSNFS forecast for February 1) but with no forcing at all

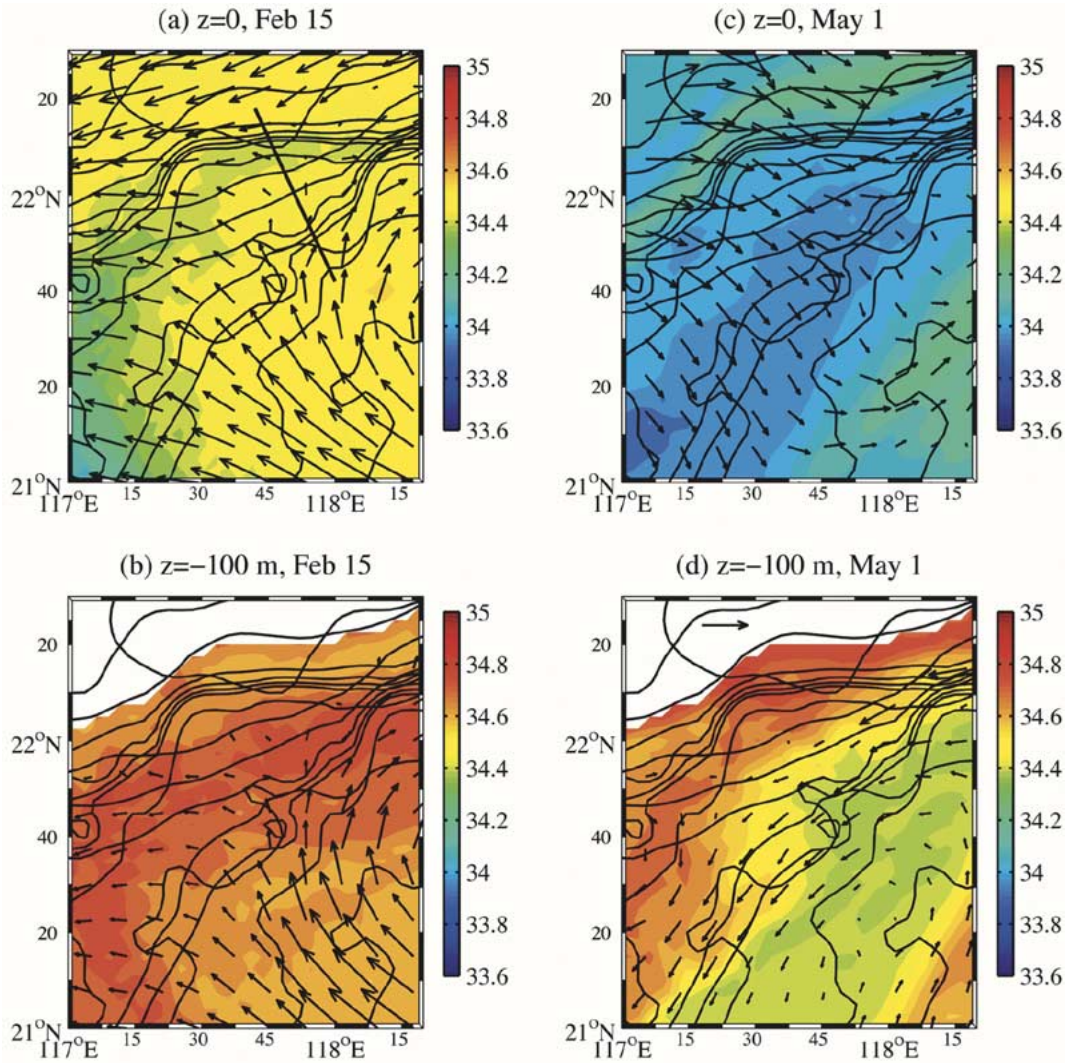

Fig. 8. Velocity vectors and salinity within the small dotted box in Fig. 1, at the surface and at 100 m depth on both February 15 and May 1 of the 2001 full-model calculation. The vector scale plotted in the white region of (d) is 0.3 ms^{-1}. Salinity scale is shown at the right in psu. Black contours show the 50, 100, 200, 300, 400, 500, 1000, 2000, 3000, and 4000 m isobaths. Black line in (a) is the location of the sections in Fig. 9. (a) $z = 0$, February 15; (b) $z = -100$ m, February 15; (c) $z = 0$, May 1; (d) $z = -100$ m, May 1.

(i.e., spindown). Then, we repeated this calculation, each time starting from the same initial condition but using an individual forcing field as the sole driving mechanism. Finally, we made several calculations starting with a resting ocean, and applying an individual forcing field as the sole driving mechanism. These results are summarized next.

A. *Spindown*

First, all of the external forcing fields described in Section II are set to zero, data assimilation is turned off and all boundaries are closed. In this calculation, the circulation within the model domain on February 1 simply spins down through frictional processes, revealing the "natural" time and space scales for the system.

Fig. 11 shows a sequence of snapshots of surface salinity and velocities, at times corresponding to those in Fig. 5. The lack of inflows through the boundaries is obvious almost immediately; the Kuroshio intrusion stops and the northern edge of the large-scale cyclonic gyre disappears. The shelf flow decays rapidly in the absence of wind forcing. The pool of salty Kuroshio water southwest of Taiwan on February 15 begins to evolve into a freely propagating baroclinic eddy, which has moved about 100 km southwestward by March 15. Its horizontal scale is several Rossby radii, consistent with geostrophic adjustment processes. Its vertical scale (not shown) is small, much like the eddy in Fig. 6. The eddy is steered by the shelf/slope topography, but it experiences little decay in strength because buoyancy shutdown prevents bottom friction from extracting much energy. Note also that the eddy drags narrow bands (streamers) of alternately fresh and salty water around its perimeter, producing quite small horizontal scales in the salinity field. By May 15, a second weaker eddy has formed off the Taiwan coast in the wake of the primary eddy. Thus, the response time scale for shelf flows is quite short (a few days), while that for the deep basin is very long (many months).

B. *Individual Forcings*

Next, model calculations were made with individual forcings to examine their influence on the circulation. The surface velocities and salinity are shown in Fig. 12 for the three most im-

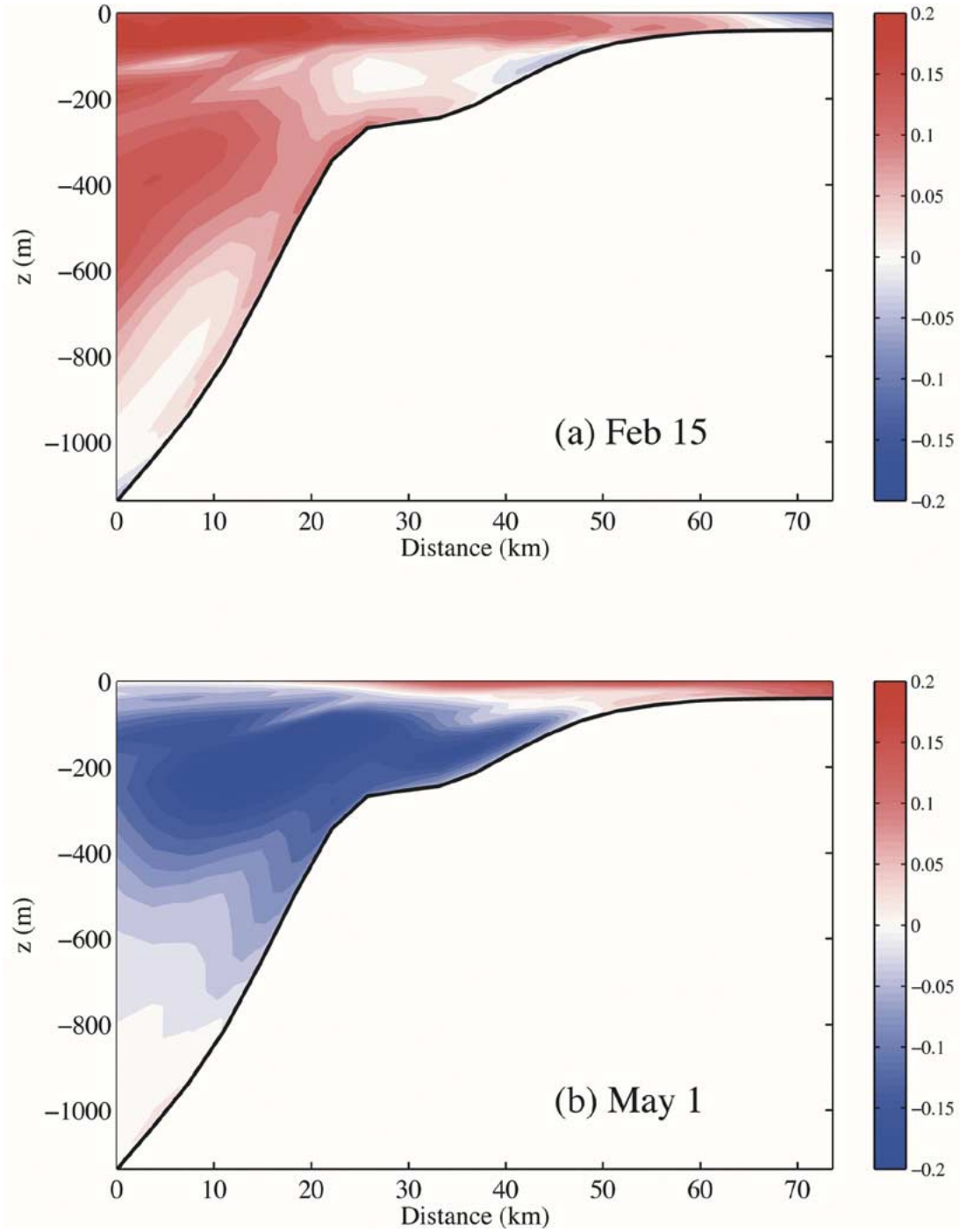

Fig. 9. Vertical sections along the black line in Fig. 8(a), showing velocity normal to the section on (a) February 15 and (b) May 1 of the 2001 full-model calculation. Scales are shown at the right in ms^{-1}. Red (blue) is out of (into) the page. White is zero velocity.

portant cases; wind forcing, open-boundary forcing and data assimilation. Each panel is a snapshot from the end of the run, on May 15, and should be compared with the full-model response in Fig. 5(d).

Wind forcing alone [see Fig. 12(a)] produces nearly uniform southwestward flow over the shelf, following the wind. The flow essentially never reverses because the wind is always from the northeast [see Fig. 2(c)], but merely weakens and becomes disorganized when the wind weakens. In the deep region, the closed boundaries prevent the large-scale cyclonic gyre from pushing the Kuroshio intrusion water toward Taiwan, so the wind is free to force the remnants of this anticyclonic eddy southwestward along the continental slope. As the anticyclonic eddy moves southwestward, a cyclonic eddy forms off the coast of Taiwan in response to both the wind stress curl described in Section III and upwelling at the closed model boundaries. Eventually, the entire deep region is filled with baroclinic eddies. The absence of the large-scale gyre eliminates the inflow of relatively fresh water, so the surface salinity remains fairly high, merely being redistributed by the wind-forced eddies.

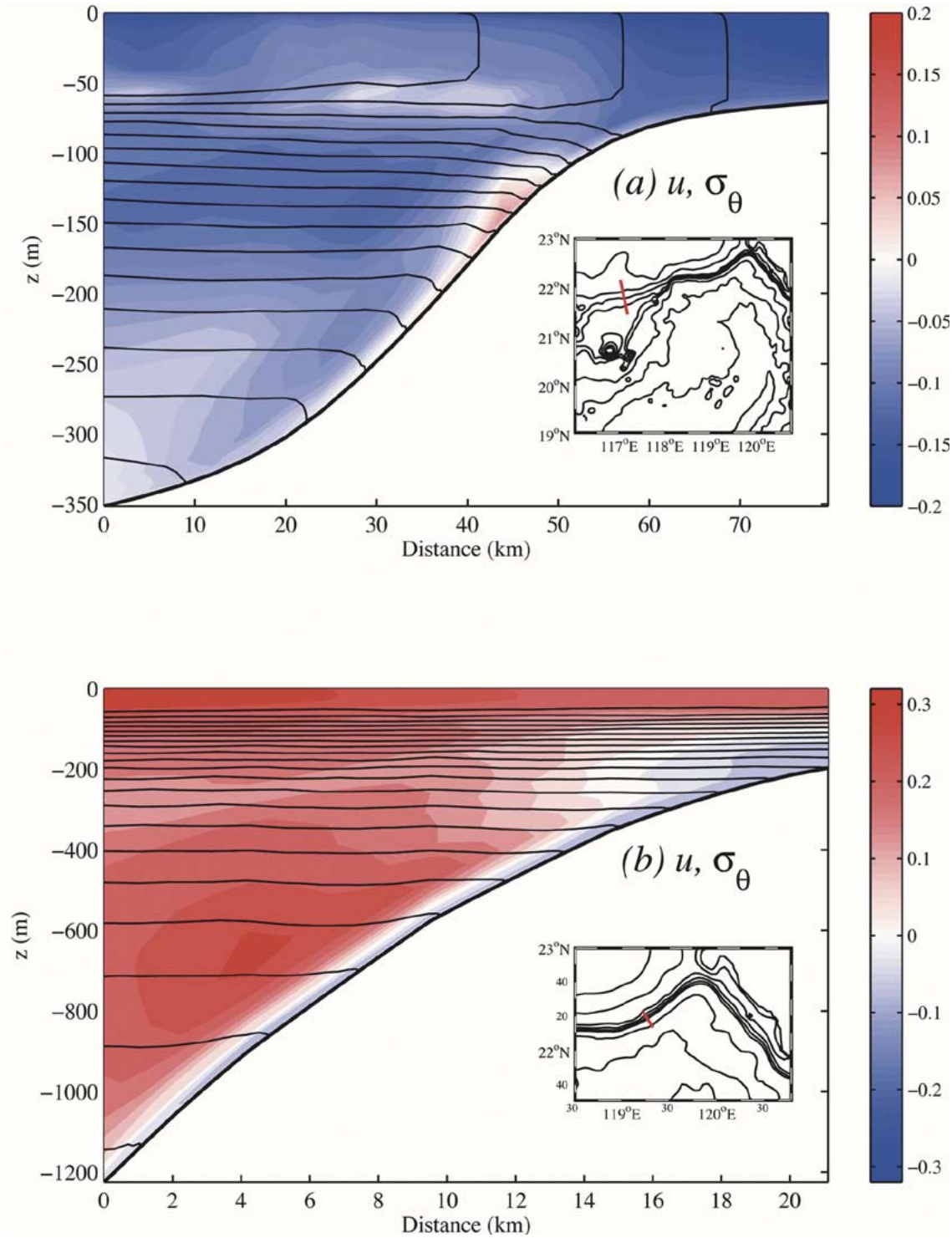

Fig. 10. Vertical sections of potential density and normal velocity along the line shown in the inset map, both on February 15 of the 2001 full-model calculation. Velocity scales are shown at the right in ms^{-1}. Red (blue) is out of (into) the page. White is zero velocity. Density contours are 23 to 27 by 0.2 kgm^{-3}.

Open-boundary forcing produces a rather different response [see Fig. 12(b)]. In this case, the circulation is dominated by the large-scale gyre at the southern boundary. The relatively fresh water penetrates farther north than in the full-model response, flowing along the shelf edge and eventually out the northern boundary. The shelf flow is strong and toward the northeast, opposite to the wind-forced shelf flow. By May 15, the remnants of the Kuroshio intrusion have been pinched between the large-scale gyre, the shelf and the Taiwan coast. This supports the conclusion of previous studies (already mentioned) that wind forcing influences the strength of the Kuroshio intrusions. That is, despite the same eastern boundary flows as in the full-model response, the absence of wind forcing allows the large-scale gyre to dominate the circulation, greatly reducing the penetration of the Kuroshio intrusion into the SCS.

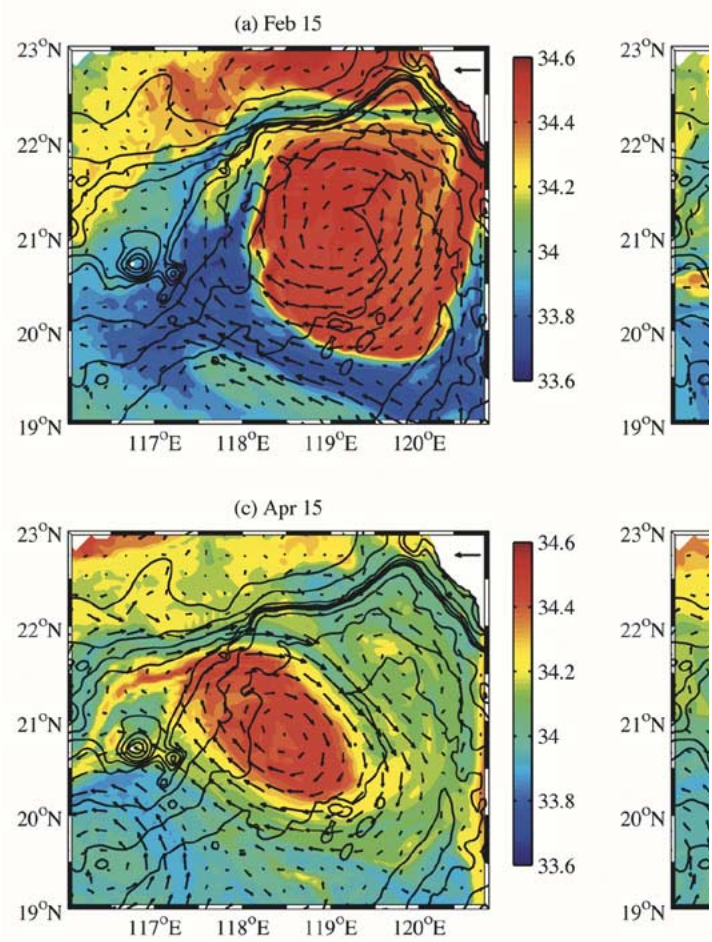

Fig. 11. Surface velocity vectors and salinity at four times during the 2001 spindown calculation. The vector scale plotted on Taiwan is 0.5 ms^{-1}. Salinity scale is shown at the right in psu. Black contours show the 50, 100, 200, 300, 400, 500, 1000, 2000, 3000, and 4000 m isobaths. (a) February 15; (b) March 15; (c) April 15; (d) May 15.

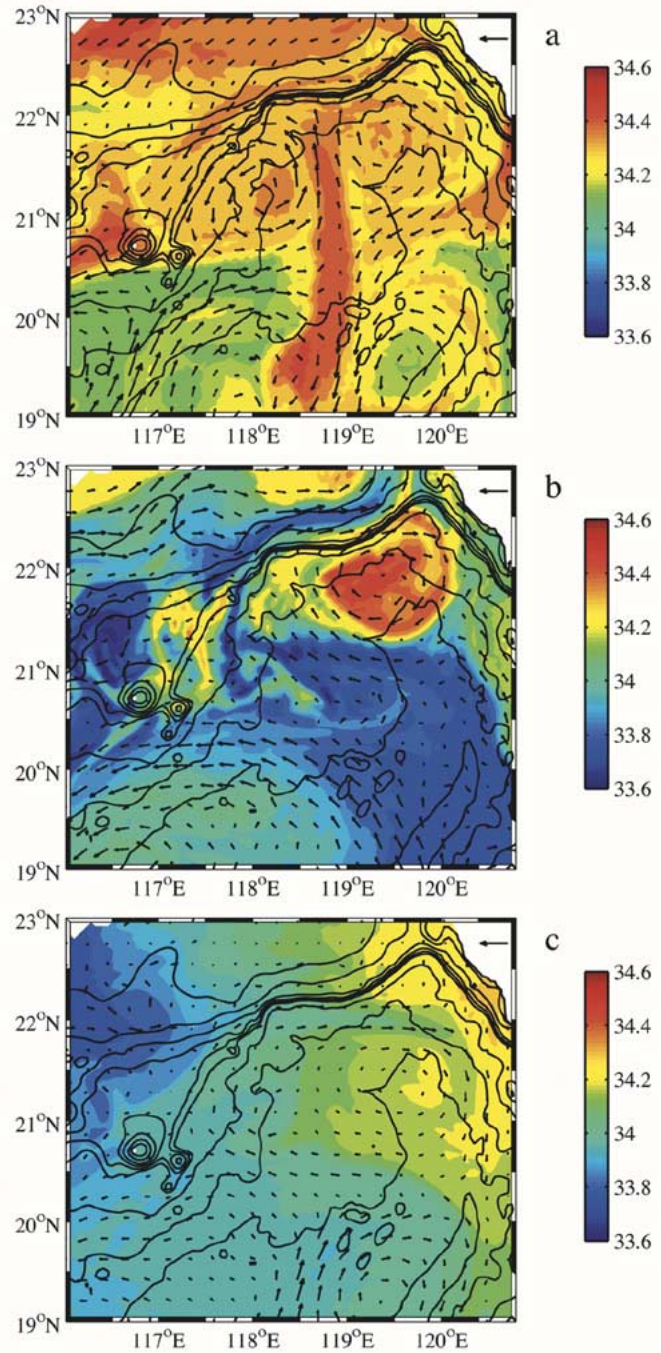

Fig. 12. Surface velocity vectors and salinity on May 15 of the 2001 calculations forced only by (a) wind stress, (b) open-boundary flows, and (c) data assimilation. The vector scale plotted on Taiwan is 0.5 ms^{-1}. Salinity scale is shown at the right in psu. Black contours show the 50, 100, 200, 300, 400, 500, 1000, 2000, 3000, and 4000 m isobaths.

Perhaps most surprising is the model response to data assimilation alone [see Fig. 12(c)]. In this case, the flow is very weak everywhere, with only a hint of an anticyclonic eddy where the Kuroshio intrusion began. Currents are, in fact, considerably weaker than those in the spindown calculation, indicating that data assimilation has had the net effect of extracting energy from the system. Thus, data assimilation seems to be damping the system, rather than driving it. This will be discussed further in Section VI.

Additional calculations were made using surface heat flux alone and air pressure alone, but these forcings had little impact on the dynamics. The surface heat flux warmed the surface, but there was no way to mix the heat downwards. Basically, the results were nearly identical to the spindown calculation described in Section V-A.

To quantify the energy input for each of the model calculations, the volume-averaged kinetic energy has been computed in the four regions (shelf, slope, upper-ocean, deep-ocean) for each model run, as done for Fig. 7. Results for each region are shown in Fig. 13. The thick solid line in each panel is the full-model response (same as in Fig. 7), while the other runs are denoted by the legend in panel (c). Over the shelf [see Fig. 13(a)], the KE decreases nearly to zero within 0.5 months for both spindown and data assimilation forcing. Wind and open-boundary forcing provide most of the KE, with the response to open-boundary forcing actually being somewhat more energetic because of the persistent northward flow at the northern boundary. Interestingly, the full-model response is more energetic than the simple sum of the wind and

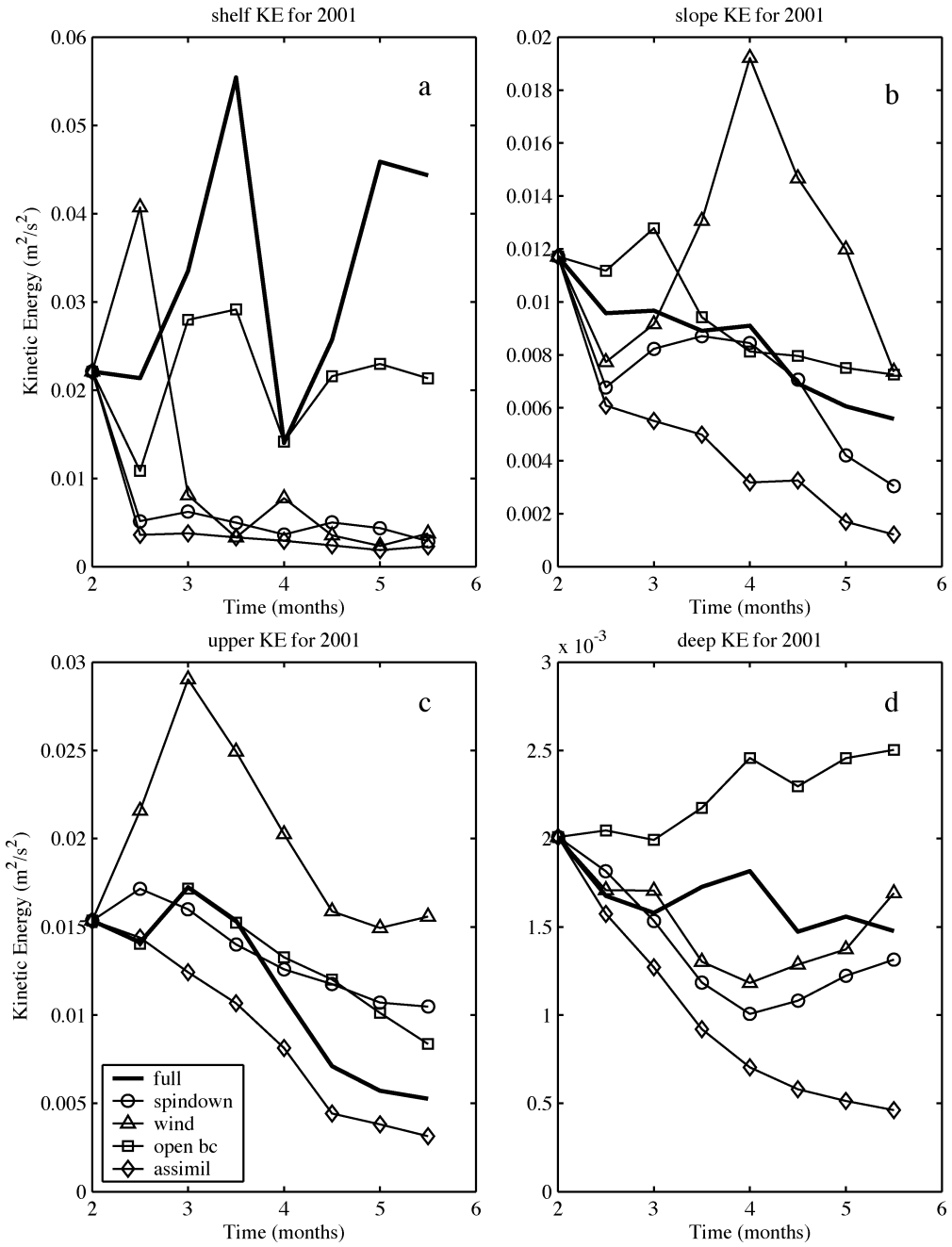

Fig. 13. Time history of the volume-averaged kinetic energy within the (a) shelf, (b) slope, (c) upper-ocean, and (d) deep-ocean regions (defined in the text) for various 2001 model calculations denoted by the legend in (c). Thick black curve in each panel shows the full-model response.

open-boundary forced responses, suggesting a strong nonlinear coupling between the two forcings, at least over the shelf. What happens is that some of the energetic slope currents are driven slightly onto the shelf in the full-model response, and this dominates the shelf KE. So, in some sense, this feature is merely an artifact of the definition of regions over which we compute KE. Over the slope [see Fig. 13(b)], the spindown response is only slightly less energetic than the full-model response. Open-boundary forcing provides energy early on, but is surpassed by the wind-forced response by mid-April. Data assimilation clearly extracts KE from the system, producing rapid decay through the entire period. In the upper-ocean region [see Fig. 13(c)], the spindown and open-boundary forcing responses are quite similar, both being slightly more energetic than the full-model response. Wind forcing is very effective at driving the upper-ocean circulation, while data assimilation again produces persistent decay. The deep-ocean region [see Fig. 13(d)] is much less energetic, with open-boundary forcing providing most of the KE. Both spindown and wind forcing lead to a general decline in KE, although not nearly as rapidly as data assimilation.

The single most obvious generalization from these calculations is that wind and open-boundary forcings provide energy to the system, while data assimilation acts to damp the

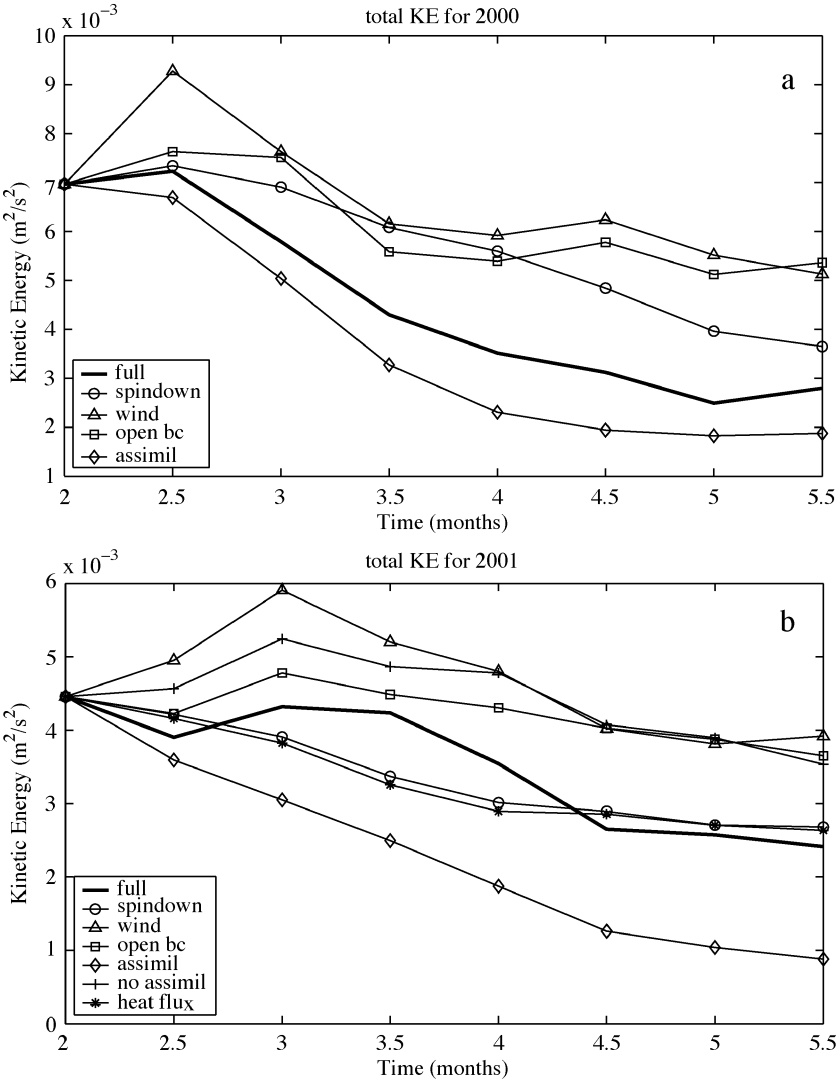

Fig. 14. Time history of the volume-averaged kinetic energy within the entire domain for various model calculations in years (a) 2000 and (b) 2001.

system. This point is further emphasized in Fig. 14, which shows the volume-averaged KE over the entire model domain for various runs in both 2000 and 2001. In both years, the full-model response is substantially weaker than that of wind forcing or open-boundary forcing. Data assimilation produces the weakest response by far. In 2000, even spindown is more energetic than the full-model response. The response to forcing by surface heat flux alone in 2001 (asterisks in panel b) is nearly identical to spindown, showing that surface heat flux is ineffective at driving currents during this time period. Finally, the response to all forcings together but no data assimilation in 2001 (pluses in panel b) is considerably more energetic than the full-model response, again showing the damping effect of data assimilation.

C. Starting From Rest

Additional model runs were made with the ocean starting from rest, driven by wind forcing and open-boundary forcing alone. These show how readily each forcing can spin up the circulation, as well as the means by which it is accomplished. In addition, a wind-forced case was run in which the curl of the wind stress was removed, and the resulting wind field was scaled so as to provide the same total energy input as the full wind field. So, the "curl-less" wind stress is spatially uniform, but it can change direction and magnitude. Here the wind-stress curl was simply computed directly from the wind-stress field.

Fig. 15 shows snapshots of surface salinity and velocities at the end of each calculation. Clearly the responses to wind forcing and to open-boundary forcing are more energetic than the response to the "curl-less" wind stress (panel b). Both wind and open-boundary forcing generate eddies, while the "curl-less" wind stress does not. However, the eddies are formed in very different ways. Open-boundary forcing imposes the Kuroshio intrusion inflow through Luzon Strait and the large-scale gyre inflow at the southern boundary that exits through the western boundary. These two flows combine, as described in Section IV, to generate the large eddy southwest of Taiwan. This circulation is similar to that shown in Fig. 12(b), but surface salinities remain relatively low because

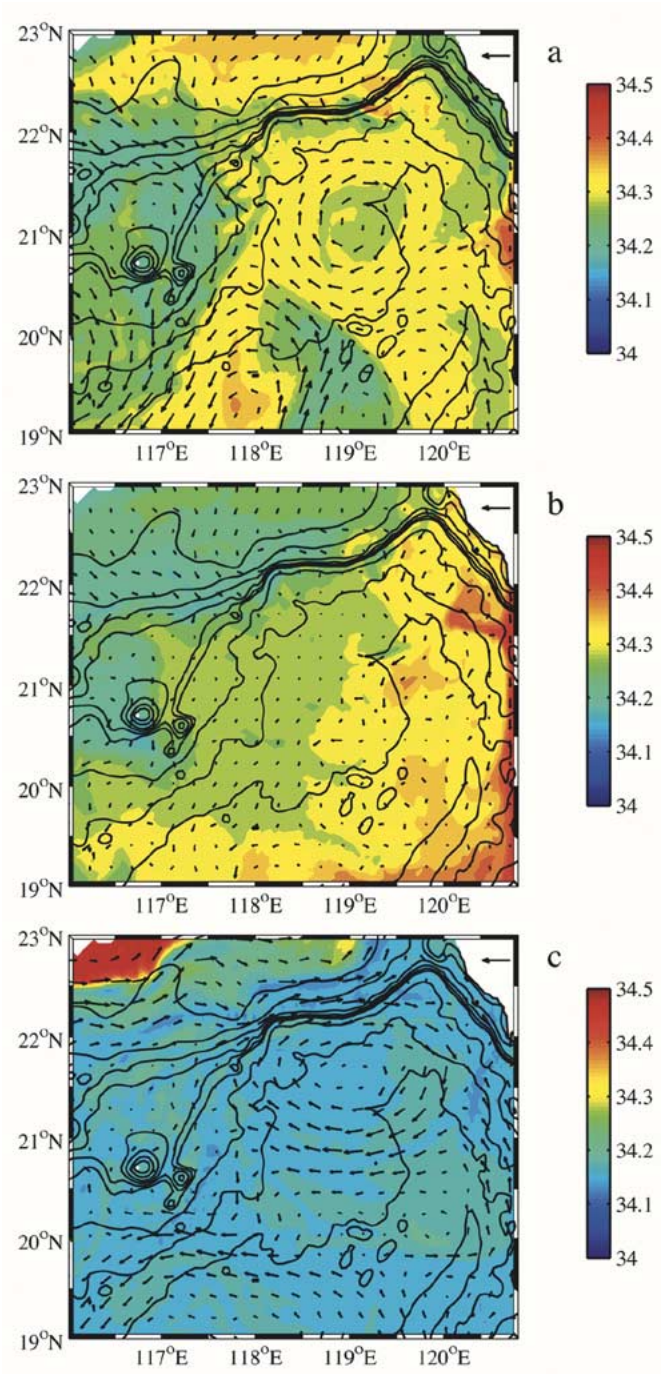

Fig. 15. Surface velocity vectors and salinity on May 15 of the 2001 calculations starting from rest and forced only by (a) full wind stress, (b) "curl-less" wind stress, and (c) and open-boundary flows. The vector scale plotted on Taiwan is 0.5 ms^{-1}. Salinity scale is shown at the right in psu. Black contours show the 50, 100, 200, 300, 400, 500, 1000, 2000, 3000, and 4000 m isobaths.

the subsurface salinity maximum (e.g., Fig. 4) remains below the surface. On the other hand, the closed boundaries in the wind-forced cases allow upwelling at these boundaries, which generates strong boundary currents and brings saltier water to the surface. (These are not readily seen in Fig. 15 because of the limited model domain shown.) Hence, the surface salinities are much higher in panels (a) and (b) than in (c). The full wind field is considerably stronger near the eastern boundary than is the "curl-less" wind, so upwelling there is correspondingly stronger with the full wind. The resulting upwelling jets are deflected westward near the southern boundary, thereby producing strong anticyclonic flow that generates the eddies in panel (a). Therefore, the wind-stress curl is not as effective at producing eddies directly as might be expected. Rather the eddies in this calculation are produced to some extent artificially by the closing of the open boundaries.

Fig. 16 shows the volume-averaged KE for each of the calculations starting from rest. The open-boundary forcing is most efficient at generating the circulation, with the full wind forcing at about half the level. The "curl-less" wind does not produce much KE. The response time scale appears to be about 0.5–1 month, with the final KE level for open-boundary forcing at about the same level as the final KE level of the full model in Fig. 14(b).

VI. Discussion and Summary

A high-resolution regional numerical model of the circulation in the northern South China Sea (see Fig. 1) reveals a complicated interaction of ocean currents over complex bottom topography. There are three primary influences on the currents in this region; 1) surface wind stress, 2) intrusions of the Kuroshio through Luzon Strait, and 3) the large-scale cyclonic gyre that occupies a large part of the northern South China Sea. Wind stress is imposed at the ocean surface, while the other two influences enter through the lateral open boundaries, based on a larger-scale North Pacific Ocean Nowcast/Forecast System. The most energetic open-boundary influences are fairly shallow features, extending no more than about 400 m deep. Currents deeper than 400 m are also primarily driven by the open-boundary flows, but they are very weak and dynamically unimportant in all of the model calculations.

Wind stress directly impacts only the upper ocean, so its effects are dominant primarily over the continental shelf, where the currents tend to follow the strong northeasterly winds of the winter monsoon. The Kuroshio intrusion typically flows westward toward the continental slope southwest of Taiwan, where it meets the large-scale cyclonic gyre that flows northward through the southern open boundary and turns westward before exiting through the western open boundary. The combination of the Kuroshio intrusion and the large-scale gyre produce an intense, narrow current directed northwest toward the continental slope, often in the region of the ASIAEX field programs. Upon reaching the slope, the current splits, with part flowing northeastward along the slope and part flowing southwestward. The details of the interaction of this jet with the sloping bottom topography are poorly understood, and have been the motivation for a recent theoretical study by Hsueh and Zhong [11]. This work advances previous theories by including a continental shelf, and suggests that most of the incoming jet should turn toward the northeast, rather than the southwest. It remains to be seen how viscous processes, including the action of the bottom boundary layer, and continuous stratification will modify these results. Unfortunately, the sensitivity of the position of the jet makes the ASIAEX field program region

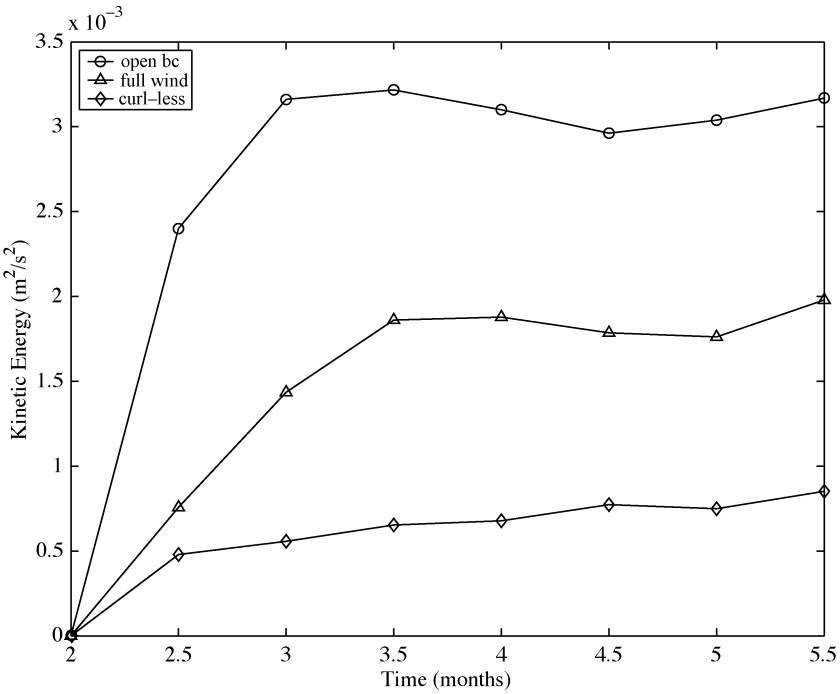

Fig. 16. Time history of the volume-averaged kinetic energy within the entire domain for three 2001 model calculations that started from rest.

particularly difficult for data-model comparisons. Slight variations in the position of the jet produce major changes in the current over the outer shelf and slope.

At the northern boundary, the model produces a persistent northward flow through Taiwan Strait into the East China Sea. This flow typically carries relatively warm, salty water from Kuroshio intrusions through the Penghu Channel just west of Taiwan, and it can dominate the shelf response, especially during times of relatively weak winds. These results are consistent with several recent studies, which have focused on the flow through Taiwan Strait (e.g., [6], [12], [13], [16]).

The NSCSNFS model appears to represent some ocean processes reasonably well. For instance, the model naturally generates large-scale eddies in the deep basin, usually the result of a Kuroshio intrusion, which adjust toward geostrophy when unforced. They are confined to the upper 300–400 m and have horizontal scales of several baroclinic Rossby radii. They tend to drift westward, riding along the steep continental slope, with little loss of energy because buoyancy advection in the bottom boundary layer shuts down the Ekman transport, thereby reducing bottom stress. The eddies wrap different water masses around them, producing narrow streamers, much like Gulf Stream warm-core rings.

The details of the flow in the northern SCS are quite sensitive to the relative strength of the three primary influences; slight variations in the strengths of the wind, Kuroshio intrusion or large-scale gyre can dramatically alter the flow in the northern South China Sea. Furthermore, the confluence of these flows at the continental slope can produce large vertical shears in the horizontal velocities and variations in water properties on short horizontal and vertical scales. Consequently, it is especially difficult to make successful forecasts. Any errors or inaccuracies in either the forcing fields or the data assimilation scheme are bound to be amplified with time, leading to the model drifting away from reality. Therefore, it is crucial that key variables be measured and inserted into the model with dynamical consistency.

Model calculations driven by individual forcings support the dominance of the three influences named above. Flow on the shelf spins down rapidly without the wind stress to drive it. Most of the energy input comes from the open-boundaries and the wind stress. Other forcings, such as surface heat flux and air pressure, have virtually no effect on the circulation, although the heat flux certainly changes the near-surface water temperature.

Perhaps the most surprising result is that the data assimilation used in the NSCSNFS model acts as a strong damper on the system, extracting energy and causing the entire system to spin down. This is caused by the low spatial and temporal resolution of the data, about 100 km and 15 days, respectively, that is assimilated compared to the model resolution (1/24°), i.e., the assimilated data have no information at the model resolution scale. Thus, the short wavelength and high frequency variations that the NSCSNFS model generates without data assimilation are filtered (i.e. damped) by the data assimilation. The same data assimilation scheme acts as an energy source for the large-scale North Pacific Basin Model. So, to improve the NSCSNFS model, emphasis should be placed on obtaining accurate winds, producing the best estimates of flow through the open boundaries and obtaining observations to be used in the data assimilation scheme that have resolution comparable to the model.

APPENDIX
DATA ASSIMILATION METHODOLOGY

The NSCSNFS assimilates three-dimensional fields of ocean temperature and salinity generated from observations of sea surface height (SSH), derived from altimetry data, and satellite derived sea surface temperature (SST). These surface observations are used to generate a full three-dimensional gridded field of ocean temperature and salinity using the Modular Ocean Data Assimilation System (MODAS) [4], [8]. A "synthetic" temperature profile is produced by projecting the surface information downward using the correlation between the steric height, the surface temperature and the subsurface temperature derived from historical profile data. Ocean salinity profiles are than derived from relationships to these temperatures at depth.

The SSH used in the calculation of these synthetic profiles is the steric height that varies in the ocean due to changes in the temperature. Altimetry data represents the total height relative to prescribed means and is modified by filtering out the barotropic signal using a relatively long mesoscale correlation time (30 days) on along track altimetry measurements. These data are processed using optimal interpolation into a two-dimensional field of SSH that is more representative of the baroclinic signal.

MODAS provides the ocean climatology of temperature and salinity that is modified by these two-dimensional fields of SSH and SST to generate the daily three-dimensional analyzes of temperature and salinity assimilated into the models. Once these analyzes are generated, they are assimilated into the model by a nudging technique defined in the following manner.

$$\mathrm{T_{update}} = \mathrm{T_{model}} + \mathrm{C_T} * (\mathrm{T_{analysis}} - \mathrm{T_{model}})$$
$$\mathrm{S_{update}} = \mathrm{S_{model}} + \mathrm{C_S} * (\mathrm{S_{analysis}} - \mathrm{S_{model}})$$

where $\mathrm{C_T}$ and $\mathrm{C_S}$ are the nudging coefficients.

The nudging coefficients include a vertical weighting function. Weighting is generally weak at the surface where temperature and salinity may change rapidly due to mixing, surface fluxes and, in shallow water, bottom stress effects. The weighting at the sea surface is zero and increases exponentially with depth over a 200 m vertical scale. The weighting is than reduced from approximately 500–1000 m depth since below 1000 m the synthetic profiles revert back to the monthly climatology or background field. At all locations, weighting is reduced exponentially to zero at the bottom over a 20 m vertical scale to reduce the influence of the data assimilation on bottom boundary layer processes.

In addition to this vertical weighting, the data are nudged into the model with a temporal weighting of $\mathrm{Dt}/\mathrm{T_{scale}} * \mathrm{R_{err}}$ where Dt is the nudging interval, $\mathrm{T_{scale}}$ is the nudging time scale (30-days to match the correlation time scale of the analysis) and $\mathrm{R_{err}}$ is the model error variance/analysis error variance. For temperature, $\mathrm{R_{err}} = 2$ or the analysis is assumed to carry twice the weight of the model and for salinity, $\mathrm{R_{err}} = 1$ as the salinity data available to generate the salinity climatology and T-S correlation was sparse.

ACKNOWLEDGMENT

The authors would like to thank K. Shearman for his assistance with parts of the analysis and plotting of results.

REFERENCES

[1] A. Blumberg and G. Mellor, "A description of a three-dimensional coastal ocean circulation model," in *Three-Dimensional Coastal Ocean Models, Coastal and Estuarine Sciences*, N. Heaps, Ed. Washington, DC: AGU, 1987, vol. 4, p. 208.

[2] S. Cai, J. Su, Z. Gan, and Q. Liu, "The numerical study of the South China Sea upper circulation characteristics and its dynamic mechanism, in winter," *Cont. Shelf Res.*, vol. 22, pp. 2247–2264, 2002.

[3] M. R. Carnes, D. N. Fox, R. C. Rhodes, and O. M. Smedstad, "Data assimilation in a North Pacific Ocean monitoring and prediction system," in *Modern Approaches to Data Assimilation in Ocean Modeling (Elsevier Oceanography Series 61)*, P. Malanotte-Rizzoli, Ed. New York: Elsevier , 1994, p. 455.

[4] M. R. Carnes, L. Mitchell, and P. W. deWitt, "Synthetic temperature profiles derived from Geosat altimetry: comparison with air-dropped expendable bathythermograph profiles," *J. Geophys. Res.*, vol. 95, pp. 17 979–17 992, 1990.

[5] S.-Y. Chao, P.-T. Shaw, and S. Y. Wu, "Deep water ventilation in the South China Sea," *Deep-Sea Res.*, vol. 43, pp. 445–466, 1996.

[6] C.-T. A. Chen, "Rare northward flow in the Taiwan Strait in winter: a note," *Cont. Shelf Res.*, vol. 23, pp. 387–391, 2003.

[7] C.-S. Chern and J. Wang, "Numerical study of the upper-layer circulation in the South China Sea," *J. Oceanogr.*, vol. 59, pp. 11–24, 2003.

[8] D. N. Fox, W. J. Teague, C. N. Barron, and M. R. Carnes, "The Modular Ocean Data Assimilation System (MODAS)," *J. Atmos. Ocean. Tech.*, vol. 19, pp. 240–252, 2002.

[9] C. Garrett, P. MacCready, and P. Rhines, "Boundary mixing and arrested Ekman layers: rotating stratified flow near a sloping boundary," *Ann. Rev. Fluid Mech.*, vol. 25, pp. 291–323, 1993.

[10] J. Hu, H. Liang, and X. Zhang, "Sectional distribution of salinity and its indiction of Kuroshio's intrusion in the southern Taiwan Strait and northeastern South China Sea late summer, 1994," *Acta Oceanologica Sinica*, vol. 18, no. 2, pp. 225–236, 1999.

[11] Y. Hsueh and L. Zhong, "A note on the deflection of a baroclinic current by a continental shelf," *Geophys. Astro. Fluid Dyn.*, vol. 97, pp. 393–415, 2003.

[12] S. Jan and S.-Y. Chao, "Seasonal variation of volume transport in the major inflow region of the Taiwan Strait: the Penghu channel," *Deep-Sea Res.*, vol. 50, pp. 1117–1126, 2003.

[13] S. Jan, J. Wang, C.-S. Chern, and S.-Y. Chao, "Seasonal variation of the circulation in the Taiwan Strait," *J. Mar. Syst.*, vol. 35, pp. 249–268, 2002.

[14] S. Jilan, "Circulation dynamics of the China Seas north of 18°N," in *The Sea: The Global Coastal Ocean Regional Studies and Synthesis*, A. R. Robinson and K. H. Brink, Eds. New York: Wiley, 1998, vol. 11, pp. 483–505.

[15] D. S. Ko, R. H. Preller, G. A. Jacobs, T. Y. Tang, and S. F. Lin, "Transport reversals at Taiwan Strait during October and November 1999," *J. Geophys. Res.*, vol. 108, no. C11, p. 3370, 2003.

[16] W.-D. Liang, T. Y. Tang, Y. L. Yang, M. T. Ko, and W.-S. Chuang, "Upper-ocean currents around Taiwan," *Deep-Sea Res.*, vol. 50, pp. 1085–1105, 2003.

[17] Z. Liu, H. Yang, and Q. Liu, "Regional dynamics of seasonal variability in the South China Sea," *J. Phys. Oceanogr.*, vol. 31, pp. 272–284, 2001.

[18] E. J. Metzger and H. E. Hurlburt, "Coupled dynamics of the South China Sea, the Sulu Sea, and the Pacific Ocean," *J. Geophys. Res.*, vol. 101, pp. 12 331–12 352, 1996.

[19] ——, "The nondeterministic nature of Kuroshio penetration and eddy shedding in the South China Sea," *J. Phys. Oceanogr.*, vol. 31, pp. 1712–1732, 2001.

[20] T. E. Rosmon, "The design and testing of the Navy Operational Global Atmospheric Prediction System," *Weather Forecasting*, vol. 72, no. 2, pp. 262–272, 1992.

[21] K. Wyrtki, "Scientific Results of Marine Investigations of the South China Sea and the Gulf of Thailand," Scripps Institution of Oceanography, NAGA Report, vol. 2, 1961.

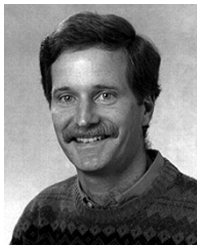

David C. Chapman received the B.S. and M.S. degrees in agricultural engineering from Cornell University, Ithaca, NY, in 1974 and 1976, respectively, and the Ph.D. degree in physical oceanography from the Scripps Institution of Oceanography, University of California, San Diego, in 1981.

He continued his oceanographic research at the Woods Hole Oceanographic Institute (WHOI), Woods Hole, MA, where he was appointed a postdoctoral investigator and moved on to the positions of Assistant Scientist, Associate Scientist, and finally to Senior Scientist in 1997. He was a world leader in coastal oceanography and made many contributions to the understanding of physical processes in oceanography. His work was of fundamental importance in understanding how coastal currents are driven by winds and river discharge. His initial work at WHOI focused on the theory of continental shelf waves. He also studied the "shelf-slope" front found along the east coast of North America by conducting a sequence of theoretical and numerical model studies that provided the first dynamically sound understanding of the shelf-slope front, how it is formed, what controls its position and strength of the along-front flow, and how the front is maintained over thousands of kilometers against dissipation. The impact of this body of work on coastal oceanography has been profound. His interest in the shelf-slope front led him to consider the behavior of freshwater plumes created by river discharge into the coastal ocean. He discovered that there is a class of buoyant plumes in which much of the plume is in contact with the bottom, and consequently the dynamics are quite different from surface-trapped plumes. In the last decade, he became a leader in modeling processes over Arctic continental shelves. His work focused on understanding the influence of bottom topography and eddy processes on the formation and spread of water made dense by surface cooling in large coastal polynyas.

Dong-Shan Ko received the B.S degree in marine science and the M.S. degree in physical oceanography from the College of Chinese Culture, Taiwan, R.O.C., in 1974 and 1979, respectively, and the M.S. degree in ocean engineering and the Ph.D.degree in applied marine physics from the University of Miami, FL, in 1981 and 1987, respectively.

He is a scientist in the Coastal and Semi-Enclosed Seas section of the Naval Research Laboratory (NRL) located at Stennis Space Center, MS. He has worked for a number of years on the development and design of the ocean nowcast/forecast systems. He has also worked with applications of ocean models for the study of circulation in deep ocean basins and in the coastal ocean. His efforts at NRL were originally focused on the development of forecast systems along the west coast of the United States and expanded to include the entire the North Pacific Ocean. He is the developer of NRL's real-time nowcast/forecast system in the Intra Americas Sea and the co-developer of the real-time nowcast/forecast system in the East Asian Seas.

Ruth H. Preller received the B.S. degree in physics from Dickinson College, Carlisle, PA, in 1975 and the M.S. and Ph.D degrees in meteorology from the Florida State University, Tallahassee, in 1979 and 1985, respectively.

She is the Superintendent of the Oceanography Division of the Naval Research Laboratory located at Stennis Space Center, MS. She is responsible for the development and design of the U.S. Navy's sea ice forecasting systems since the mid-1980s. She has also worked with applications of ocean models to the circulation of both coastal and semi-enclosed seas. Her group has developed ocean forecast systems for the western Pacific called the East Asian Seas Nowcast/Forecast System and for the Gulf of Mexico and the Caribbean called the Intra Americas Sea (IAS) Nowcast/Forecast System. These forecast systems are nested within the Navy's Global NCOM forecast system. She and her team are responsible for the development of the PCTides globally relocatable system for tidal height prediction. She served as an Associate Editor for High Latitude Oceanography publications in *The Journal of Geophysical Research Oceans* and then as the Editor for this topic area for over nine years.

Dr. Preller serves on several national scientific committee and has interacted with the international science community having served as the session chairman or organizer of various science conferences including the annual Operational Oceanography session of the European Geophysical Union conference.